# Characterizing the 2019-2021 Drought in Southern and Southeastern Brazil Using S-TRACK Method

Osmar Toledo Bonfim *, Vanessa Ferreira , Rafael Maroneze , Roilan Hernández Valdes , Luca Mortarini

Posted Date: 9 January 2024

doi: 10.20944/preprints202401.0746.v1

Keywords: Precipitation Deficit; Drought indexes; Spatial tracks; South America.

*Article*

# Characterizing the 2019–2021 Drought in Southern and Southeastern Brazil Using S-TRACK Method

**Osmar Toledo Bonfim [1,*], Vanessa Ferreira [2], Rafael Maroneze [3,*], Roilan Valdes [4] and Luca Mortarini [5]**

[1] Universidade Federal do Pampa - campus Alegrete ; osmarbonfin@unipampa.edu.br
[2] Universidade Federal do Pampa - campus Alegrete; vanessaferreira@unipampa.edu.br
[3] Universidade Federal do Pampa - campus Alegrete; rafaelmaroneze@unipampa.edu.br
[4] ENGIE Brasil Energia ; roilan.valdes@engie.com
[5] Institute of Atmospheric Sciences and Climate; l.mortarini@isac.cnr.it
* Correspondence: osmarbonfin@unipampa.edu.br (OTB); rafaelmaroneze@unipampa.edu.br (RM)

**Abstract:** The period from 2019 to 2021 witnessed an enduring and severe drought that impacted southeast South America. Initially characterized as a meteorological drought, its influence later extended across the entire hydrological cycle. This paper explores the application of the S-TRACK method to monitor and characterize the 2019/21 drought in Southern Brazil (SB) and Southeast Brazil (SEB). Monthly precipitation data from reanalyses and satellites, alongside the Standardized Precipitation Index (SPI) for drought quantification, are utilized. Precipitation datasets, validated against rain gauge records, highlight ERA-5 and CHIRPS as having the highest correlation in both SB and SEB, with PERSIANN exhibiting a moderate correlation. The utilization of the S-TRACK method for spatial drought tracking revealed the temporal dynamics of the drought events, with three significant episodes occurring in 2020/2021. Initially, the onset of the drought was observed in the SB region, characterized by intensities ranging from moderate to extreme. Subsequently, the drought extended northward, reaching its maximum intensity at lower latitudes within the SEB region before either dissipating or experiencing a reduction in both its spatial extent and intensity. The prolonged presence of drought-affected areas in the same region over an extended period contributed significantly to the exacerbation of drought severity, particularly during the March to May trimester.

**Keywords:** precipitation deficit; drought indexes; spatial tracks; South America

## 1. Introduction

During the period from 2019 to 2021, a prolonged and intense drought affected the southeast South America region. The event initially manifested as a meteorological drought characterized by precipitation deficits, but its persistence also impacted the entire hydrological cycle, profoundly affecting soil moisture, rivers, surface and groundwater reservoirs, as well as regional ecosystems. The effects of this event were widespread, generating significant repercussions in agricultural production, water supply, energy generation, and posing a serious threat to vital ecosystems [1–3]. For instance, in the Southern Brazil (SB) and Southeast Brazil (SEB) regions, significant agricultural losses were recorded. Simultaneously, a notable decline in discharge levels in vital rivers, including the Iguaçu, Uruguay, and Paraná rivers, has resulted in limitations affecting both hydropower generation and freshwater supply [4].

Drought monitoring indices, such as the Standardized Precipitation Index (SPI), play a fundamental role in identifying precipitation scarcity and tracking the development of drought conditions in specific locations. The significance of SPI in drought analysis cannot be underestimated, as it is a valuable tool for quantifying and characterizing the severity of drought conditions and providing information about the spatial extent of these events [5,6]. However, there is still a lack of

Preprints (www.preprints.org) | NOT PEER-REVIEWED | Posted: 9 January 2024 doi:10.20944/preprints202401.0746.v1



consistent procedures for continuously tracking drought-affected areas, which, in turn, hinders the assessment of the temporal variations that comprise the spatiotemporal dynamics of this climatic phenomenon.

The spatial drought tracking method, known as S-TRACK, emerges as a highly relevant tool in the context of drought analysis and prevention. By providing a comprehensive perspective in both spatial and temporal terms, S-TRACK enables a deeper understanding of how droughts form, move, and intensify over time, allowing for a more accurate assessment of the risks associated with these extreme climatic events [6,7].

Ref. [8,9] conducted studies using the S-TRACK methodology to analyze the spatial characteristics of drought and created trajectories to investigate its spatiotemporal dynamics. These trajectories provided information on the duration, severity, and intensity of drought conditions in Iran and southern Australia, respectively. The results of these studies offer valuable insights that can contribute to the enhancement of preparedness for extreme precipitation events as they become more frequent. Furthermore, they provide authorities and local communities with the opportunity to take proactive measures to mitigate the impacts of droughts.

This study focuses on the identification and characterization of the areas affected by the 2019/21 drought in SB and SEB, highlighting the contribution of the S-TRACK method in investigating this phenomenon and how its application enables a characterization of this drought event.

## 2. Materials and Methods

### *2.1. Datasets and study area*

The study area includes the Southern (SB) and Southeastern (SEB) regions of Brazil, demarcated by the geographical coordinates 14°15' to 33°45' latitude South and 39°40' to 57°37' longitude West (Figure 1). These regions exhibit substantial geographical diversity and occupy a vast territorial expanse. Cumulatively, they encompass an area of approximately 1.682.676 km², representing approximately 20% of the Brazilian territory.

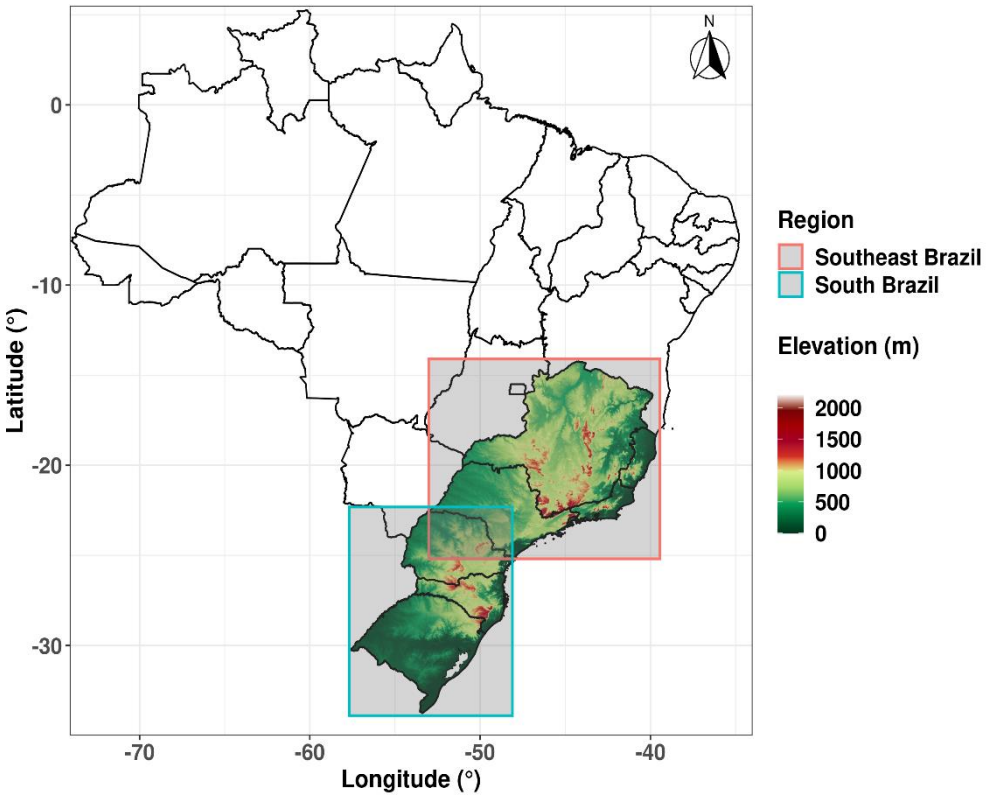


**Figure 1.** Topographic features and location of the Southeast and South regions of Brazil.

Preprints (www.preprints.org) | NOT PEER-REVIEWED | Posted: 9 January 2024 doi:10.20944/preprints202401.0746.v1



To identify areas experiencing dry conditions in the Southern and Southeastern regions of Brazil during the 2019/2021 period, monthly precipitation data were utilized. Given the limited spatial and temporal resolution of meteorological stations in Brazil, precipitation data from reanalyses and satellites were selected due to their higher resolution, providing a significant advantage, especially in terms of area coverage in regions with limited data availability. The selection of datasets was based on two key criteria: good spatial resolution and data availability, resulting in the choice of three distinct datasets.

Two of the datasets were obtained through satellite-based methods. The first one is the Precipitation Estimation from Remotely Sensed Information using Artificial Neural Networks Climate Corrected and Continuous Distributed (PERSIANN-CCS-CDR) system, featuring a spatial resolution of 0.04° and a temporal resolution of half an hour [10]. The second dataset is the Climate Hazards Group Infrared Precipitation with Stations (CHIRPS), comprising a high-resolution (0.05°) precipitation dataset that integrates multiple sources, including NOAA, CPC, NCDC, and meteorological station data [11].

The third dataset consists of precipitation information obtained from ERA-5, the fifth generation of atmospheric reanalysis developed by the European Centre for Medium-Range Weather Forecasts (ECMWF). ERA-5 provides hourly precipitation data with a spatial resolution of 0.25°, along with an extensive and consistent climatic record covering the entire globe [12].

To validate the precipitation estimates derived from these datasets, historical precipitation data series from the National Institute of Meteorology (INMET) were used. A period of 30 years (1991-2020) was chosen for analysis, as it is considered suitable for climatological statistical analyses.

### *2.2. Drought characterization*

In order to quantify and characterize the extreme drought event, the Standardized Precipitation Index (SPI) was employed at a 3-month scale. Previous studies [13,14] have highlighted that the SPI is more consistent in representing actual drought conditions when applied at shorter and medium time scales, compared to longer scales. The SPI is a simple, flexible, and effective index that allows for the analysis of both wet and dry periods, relying solely on precipitation as the input parameter [15–17].

The SPI is computed based on the accumulated probability of occurrence for each monthly precipitation value. To standardize the data, the Z value is calculated by subtracting the monthly precipitation value P$i$ from the mean precipitation of the corresponding period $i$, and dividing the result by the standard deviation σi. As demonstrated by the following equation 1:

$$SPI = Z_i \frac{P_i - \underline{P_i}}{\sigma_i} \quad (1)$$

The SPI is a standardized indicator that adjusts the precipitation to a statistical distribution over a reference period, enabling the classification of drought and wet conditions using a simple scheme based on standard deviations from the mean. It facilitates the comparison of precipitation magnitude across different locations and time periods, offering an objective measure of precipitation events. Positive SPI values indicate wet periods, while negative values represent rainfall deficits. Table 1 presents the SPI categories, as defined by [15].

**Table 1.** Classification of dry and wet periods according to the SPI value [15].

| SPI | Category |
|---|---|
| Extreme wet | > 2 |
| Severe wet | > 1,5 to ≤ 2 |

Preprints (www.preprints.org) | NOT PEER-REVIEWED | Posted: 9 January 2024 doi:10.20944/preprints202401.0746.v1



| | |
|---|---|
| Moderate wet | > 1 to ≤ 1,5 |
| Near normal | > -1 to ≤ 1 |
| Moderate dry | > -1,5 to ≤ -1 |
| Severe dry | > -2 to ≤ 1,5 |
| Extreme dry | ≤ -2 |

*2.3. Validation of precipitation datasets*

The methodology proposed by Ref. [18] was employed to evaluate the accuracy of satellite data (CHIRPS, PERSIANN) and reanalysis data (ERA-5) in terms of the spatial distribution of precipitation in the SB and SEB regions. The analysis was based on the temporal series of 3-month SPI (SPI-3) from 1991 to 2020, using observations from INMET meteorological stations as the reference data. The Taylor diagram, introduced by Ref. [18] and employed by Ref. [19], offers a concise statistical summary of the agreement between the estimated and observed patterns. This graphical representation considers the correlation coefficient (R), standard deviation amplitude (σ), and Root Mean Square Error (RMSE) as evaluation metrics. It provides an overview of how well the simulated pattern approximates the observed data.

However, relying solely on the correlation coefficient (R) is insufficient to determine whether two variables share the same range of variation, as it does not account for factors such as variances. To assess the quality of the model and quantify the disparity between two variables, the most commonly utilized statistic is the root mean square difference (E), given by equation 2:

$$E = \left[\frac{1}{N}\sum_{n=1}^{N}(f_n - r_n)^2\right]^{\frac{1}{2}} \quad (2)$$

where: ($E$) represents the root mean square difference, ($n$) is the number of data points, ($f_n$) and ($r_n$) are the corresponding values of the two variables being compared.

The root mean square difference provides a measure of the average discrepancy between the observed and predicted values, allowing for a comprehensive evaluation of the model's performance. It takes into account both the magnitude and direction of the differences, providing valuable insights into the accuracy and fit of the model.

The construction of the Taylor diagram entails representing either a half or quarter circle, with the quarter circle being the more commonly used representation. The x and y axes correspond to the measures of σ, where the σ value of the observed data is depicted along the x-axis. The azimuth from the origin to the model is proportionate to the correlation coefficient (R). The distance between the reference point on the diagram and the model point is represented by the value of the root mean square difference (E).

*2.4. Spatial Tracking of Drought*

In terms of drought spatial dynamics, commonly used drought monitoring indices like the SPI offer insights into the spatial extent and intensity of drought events. However, analyzing the spatial distribution of drought at a specific moment lacks the ability to capture the spatiotemporal patterns of drought over time, hindering the assessment of the temporal variations that contribute to their spatiotemporal dynamics [6].

To overcome this limitation, the Spatial Tracking of Drought (S-TRACK) method was introduced by Ref. [7,20], and subsequently enhanced by other researchers [6,8,9,21]. S-TRACK aims to construct

Preprints (www.preprints.org) | NOT PEER-REVIEWED | Posted: 9 January 2024 doi:10.20944/preprints202401.0746.v1



spatial tracks and trajectories of drought, thereby enhancing the monitoring capabilities. The S-TRACK method involves three key steps: (1) computation of spatial drought units, also known as areas or clusters; (2) determination of the centroids for these spatial drought units; and (3) establishment of connections between the centroids in the spatiotemporal domain.

Within the spatial context, drought units are identified through cluster analysis following the application of SPI. To assess whether a cell is experiencing drought, a binary approach is employed, assigning a value of 1 to indicate drought presence and 0 to indicate its absence. This binary representation enables the utilization of pattern recognition techniques that group neighboring cells based on shared characteristics [22]. As demonstrated by the following equation 3:

$$D_S = \{1 if SPI_t \leq L \vee 0 if SPI_t > L\} \quad (3)$$

Where $D_s$ represents the drought state in each cell at every time step ($t$), based on the designated threshold ($L$).

During this step, the threshold value ($L$= -1) [5,15] was used to evaluate the occurrence of drought at each grid point. Once the clusters are identified, the largest cluster is chosen, and its corresponding centroid is computed at each time step (t) [6,8]. This characteristic facilitates determining the geographic location of each drought area and tracking its temporal movement by connecting the centroids across consecutive time instances, resulting in the formation of drought tracks that represent the trajectory of the drought.

For the process of connecting the centroids, parameters a, b, c, and d were established following the description provided by Ref. [21].

$$A_t \geq a = True$$

$$A_t < b = True$$

$$\Delta l \leq c = true(clustersconnected)$$

or

$$A_t > b = false$$

$$\Delta l \leq d = true(clustersconnected)$$

Where parameter ($a$) must be less than or equal to the 50th percentile of the area of the largest cluster ($A$), while parameter ($b$) must be greater than or equal to the 50th percentile of the area ($A$). On the other hand, parameters ($c$) and ($d$) represent the 70th percentile of the distance between centroids ($\Delta l$). Parameters (a) and ($b$) are considered as percentiles of the drought area, while parameters ($c$) and ($d$) represent percentiles of the distance between centroids [21].

Drought tracking enables the identification of trajectories with defined starting and ending points, providing insights into their main direction. The initial and final locations are determined based on the centroids of the first and last clusters, respectively. The magnitude, or extent, of the drought encountered at each time interval using the S-TRACK method is quantified as a measure, calculated by summing the drought areas over time ($t$). Additionally, the intensity of the drought is defined by the most frequent category of the SPI at the given time ($t$).

## 3. Results

In order to assess the accuracy of precipitation estimates derived from PERSIANN, CHIRPS, and ERA5 in comparison to observed data obtained from INMET meteorological stations, Taylor diagrams were employed to analyze SPI-3 time series in the Southern Brazil (SB) and Southeast Brazil (SEB) regions. The findings, depicted in Figure 2, indicate that the estimated data for SB demonstrated more variability, as evidenced by relatively elevated standard deviation values. In terms of correlation (r), the ERA-5 and CHIRPS estimates exhibited the highest magnitudes, approximately 0.90, indicating a very strong correlation. On the other hand, the correlation performance of PERSIANN was found to be moderate, falling below 0.70.

Preprints (www.preprints.org) | NOT PEER-REVIEWED | Posted: 9 January 2024 doi:10.20944/preprints202401.0746.v1



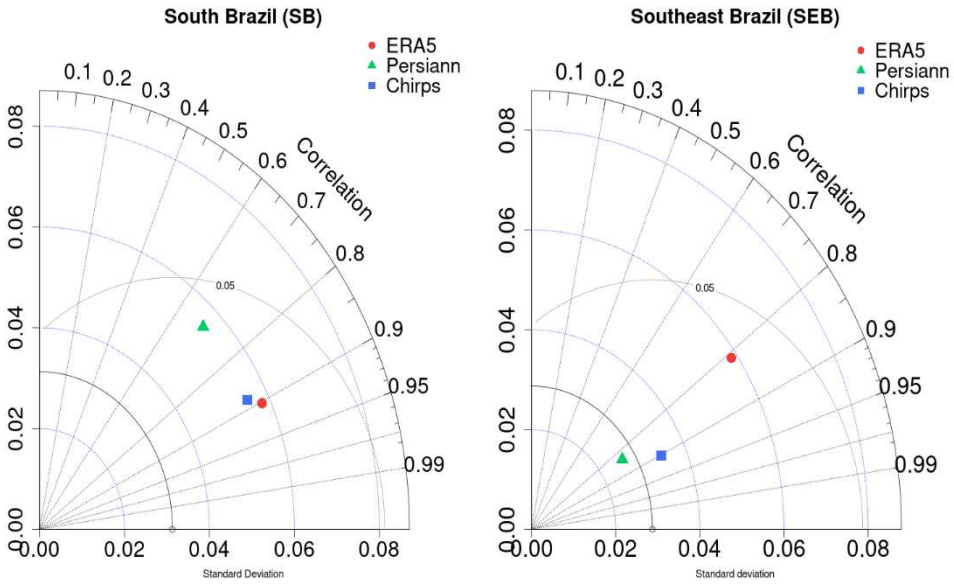


**Figure 2.** - Taylor diagrams comparing the SPI-3 time series of CHIRPS, PERSIANN, and ERA-5 products with respect to the observed data obtained from INMET meteorological stations for the period of 1991-2020.

The Taylor diagram analysis for SEB demonstrated that the PERSIANN and CHIRPS satellite datasets exhibited the best agreement with the observed data from INMET, as indicated by their similar standard deviations and strong correlations. The correlation coefficient for PERSIANN exceeded 0.80, indicating a strong correlation, while the correlation for CHIRPS was approximately 0.90, denoting a very strong correlation. In contrast, the ERA-5 data showed higher standard deviation values, indicating greater variability in the SEB region. Nevertheless, it still maintained a strong correlation above 0.80. Additionally, the root mean square error (RMSE) values for both regions (SB and SEB) were below 0.05, indicating a good performance of the estimated data in accurately predicting the observed values.

These findings align with the results reported by Ref. [23], demonstrating that CHIRPS exhibits greater accuracy in representing the spatial distribution of monthly precipitation compared to PERSIANN. Additionally, other studies including [24–26] have similarly reported comparable correlation values between the estimated precipitation data and observations obtained from meteorological stations.

Figure 3 presents the spatial representation of drought conditions and their severity in the SB and SEB regions. The three spatiotemporal drought distribution maps (Figures 3(A) ERA-5, 3(B) CHIRPS, and 3(C) PERSIANN) exhibited consistent results in identifying the drought event throughout the year 2020. During the December 2019 to February 2020 (DJF) trimester, the SPI-3 maps derived from ERA-5 data revealed an extreme drought occurrence in the southernmost region of SB. However, this extreme drought condition was less pronounced in the CHIRPS and PERSIANN datasets, which categorized it as severe and moderate drought, respectively, covering a smaller proportion of the area.

Preprints (www.preprints.org) | NOT PEER-REVIEWED | Posted: 9 January 2024 doi:10.20944/preprints202401.0746.v1



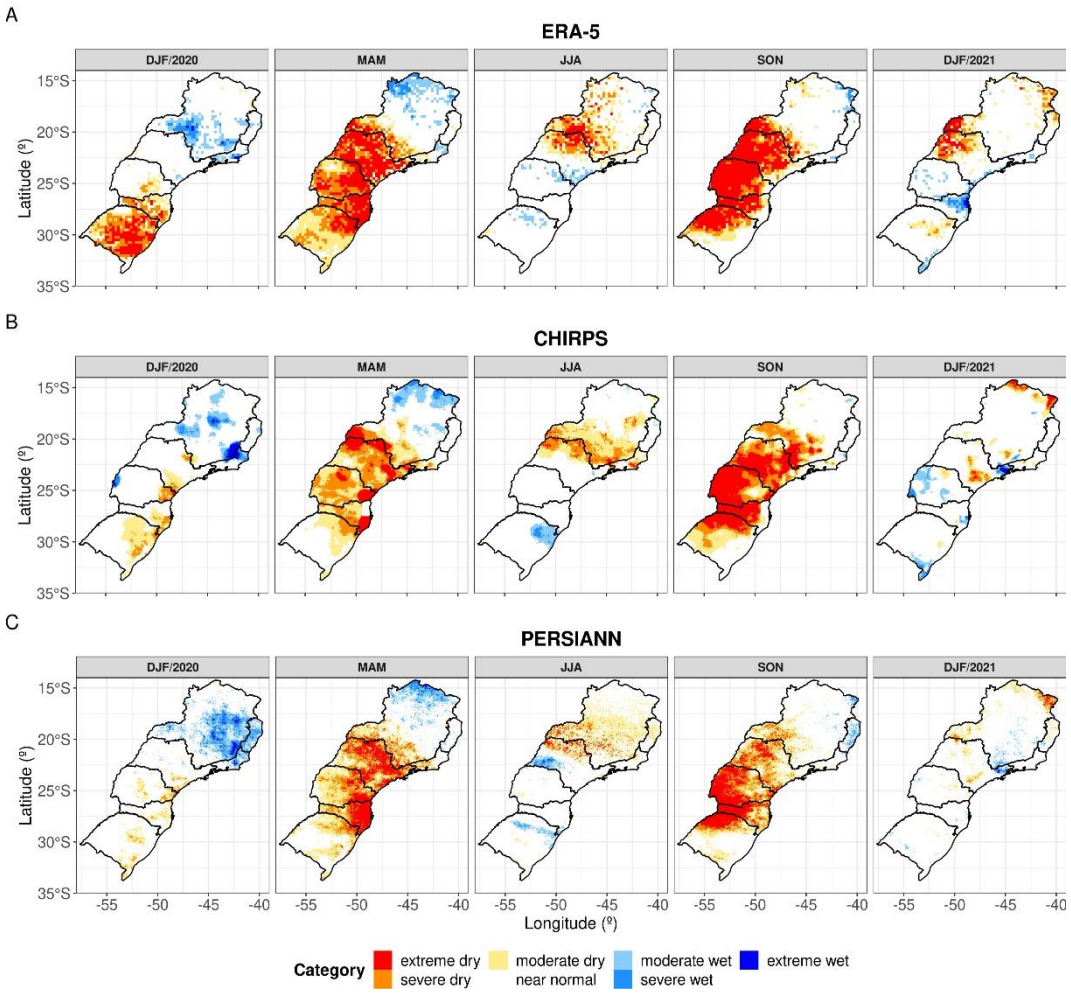


**Figure 3.** - Spatial-temporal distribution of meteorological drought in the South and Southeast of Brazil throughout 2019-2020 using SPI-3. (**A**) ERA-5; (**B**) CHIRPS; (**C**) PERSIANN.

During the March to May (MAM) and September to November (SON) trimesters of 2020, the occurrence of extreme drought was primarily concentrated in the central region of the study area, with a greater impact on states located between latitudes 20°S and 30°S. This spatial pattern was consistently observed across the three datasets analyzed. Specifically, in the state of Minas Gerais, the southern region experienced a more severe drought during both trimesters, while the northern part of the state was classified as relatively humid. This behavior can be attributed to the fact that the SEB is located in a transitional zone of the El Niño-Southern Oscillation (ENSO) phenomenon [27,28].

The increasing demand for water resources and the occurrence of droughts in recent years emphasize the need for a comprehensive understanding of the nature and extent of these events. Consequently, it is crucial to establish consistent methodologies that enable the assessment of spatio-temporal drought conditions. To address this gap, the S-TRACK methodology [6,8,9,21] was implemented using the average of the three dataset to evaluate spatiotemporal drought conditions. The results, presented in Figure 4, demonstrate the spatial tracking of drought in the SB and SEB regions, revealing the occurrence of three events in 2020/2021, the first two originating in the SB region and the third in the SEB region.

During the November to January (NDJ - 2019/2020) trimester, the onset of the drought event was observed near latitude 30°S with a moderate intensity. Subsequently, the event advanced northward and reached its peak magnitude and intensity during the MAM trimester near latitude 25°S, being classified as an extreme drought. The persistence of centroids in this region suggests that drought conditions remained stationary for an extended period, contributing to the aggravation of drought severity, particularly during the MAM trimester. This is corroborated by the spatial SPI maps (Figure

Preprints (www.preprints.org) | NOT PEER-REVIEWED | Posted: 9 January 2024 doi:10.20944/preprints202401.0746.v1



3), which indicate an expansion and intensification of drought in the SB region between DJF and MAM.

The drought centroid subsequently shifted further north and settled near latitude 20°S, characterized as a moderate drought. Finally, the drought dissipated during the July to September (JAS) trimester. The drought persisted in a stationary position near 20°S for an extended period, leading to an intensification of its severity during the JJA and JAS trimesters, as depicted in Figure 3. These observations are consistent with the findings of Ref. [8], who suggested that the persistence of large drought areas in the same region over time could contribute to the severity of droughts during periods characterized by intense drought events.

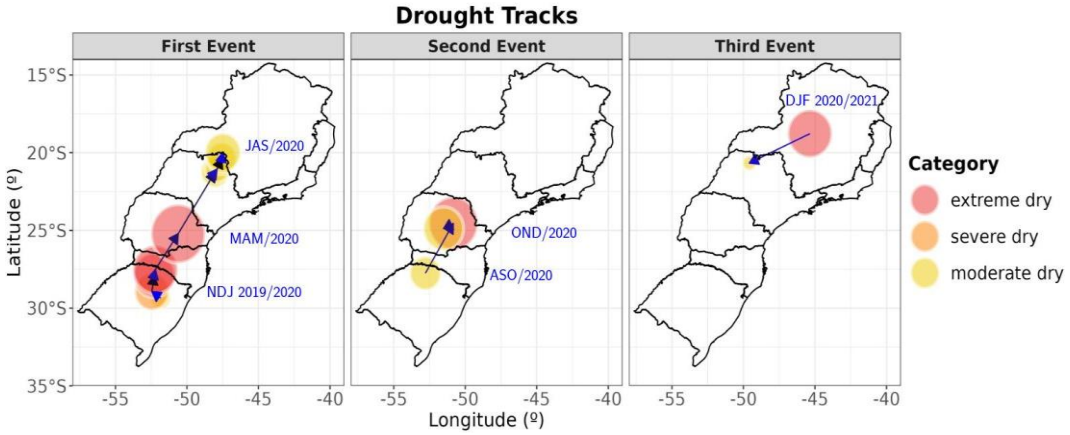


**Figure 4.** - Spatial tracking of drought calculated based on the distance from the centroid of the largest drought cluster in each quarter of 2020. The size of the circle represents the spatial extent of drought, while the color indicates the intensity. The first event occurred in the NDJ 2019/20 quarter and extended until JAS. The second event began in ASO to OND 2020, and the Third event occurred in the NDJ 2020/21 to DJF 2020/21.

During the August to October (ASO) trimester, the second drought event initiated near latitude 27°S with a moderate intensity. In the following trimesters, the drought episode advanced northward and intensified during the SON trimester near latitude 25°S, resulting in an extreme drought classification. Subsequently, the drought event experienced a slight southwest displacement and diminished in intensity, transitioning back to a moderate drought classification. The third event initiated in the November to January (NDJ - 2020/2021) trimester at approximately 19°S latitude, displaying SPI-3 values within the extreme drought category. However, as the drought event progressed westward, its intensity diminished and dissipated during the subsequent trimester (DJF - 2020/2021). In the first event, the drought propagated over a distance of approximately 1200 km, whereas in the second and third event, its trajectory extended across approximately 500 km.

Figure 5 presents the spatial coverage of drought occurrence throughout the year 2020, quantified by the percentage of the SB and SEB area with SPI-3 values ≤ -1, considering the three datasets. The MAM trimester exhibited the most extensive spatial coverage of drought, with approximately 70% of the area affected in the ERA-5 dataset and around 60% in the satellite datasets. In contrast, the May to July (MJJ) trimester had the lowest percentage of area affected by drought, with approximately 15% in all three datasets. Subsequently, there was an increase in the percentage of area affected by drought, reaching around 60% again during the SON trimester, particularly in the CHIRPS dataset.

Preprints (www.preprints.org) | NOT PEER-REVIEWED | Posted: 9 January 2024 doi:10.20944/preprints202401.0746.v1



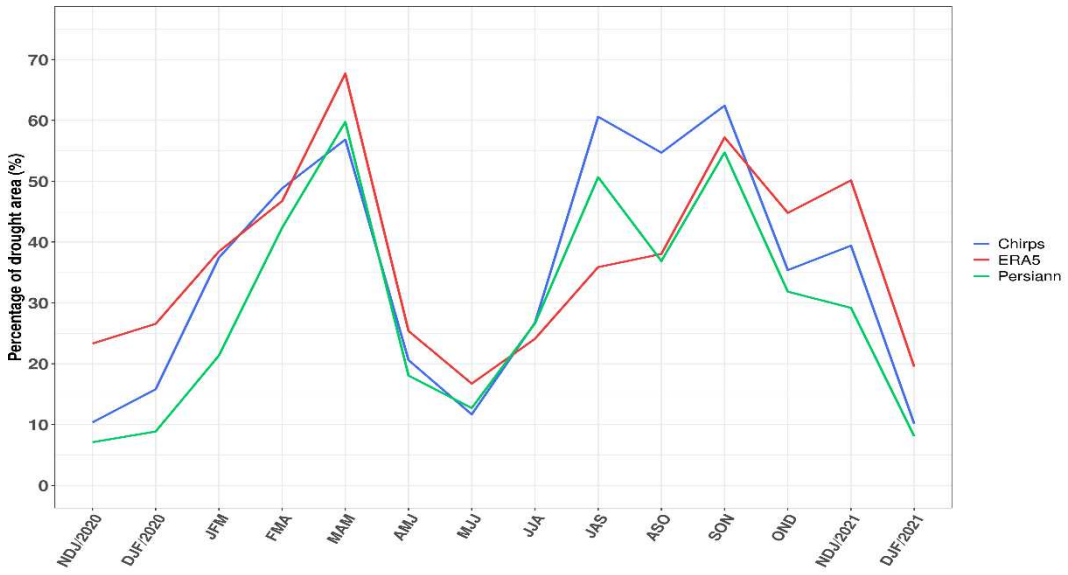


**Figure 5.** - Percentage of the area in the South and Southeast regions affected by drought events (SPI-3 ≤ -1) throughout 2020.

According to Ref.[2], during the MAM period of 2020, the drought in the central-southern region of Brazil led to a deficit of 267 km³ in water storage compared to the 20-year seasonal average. This water scarcity affected various components of the hydrological system, including rivers, lakes, soil, and aquifers. Furthermore, a significant number of major reservoirs recorded capacities below 20%, leading to significant impacts, particularly in agriculture, energy production, and the provision of potable water to the population.

As reported by [1], the agricultural sector in the SB region states suffered substantial losses, with more than 40% of the area being affected. The National Center for Monitoring and Natural Disaster Alerts documented that reservoirs reached their lowest levels in April 2020, resulting in consequences for hydropower generation and water supply, particularly in the southern states of Brazil. Notably, hydroelectric power plants situated along the Paraná and Iguaçu rivers recorded their lowest historical storage levels during this period [29].

Recent studies [4,30] have examined the 2019-2021 drought event in South America, focusing on various affected regions and the combination of climate factors and atmospheric conditions that contributed to the dry conditions, particularly in 2020. The Indian Ocean Dipole (IOD), Pacific Decadal Oscillation (PDO) in a negative phase, and Atlantic Multidecadal Oscillation (AMO) in a positive phase were identified as factors contributing to the extreme dry conditions.

Furthermore, research by [31] revealed that southeast South America experienced precipitation deficits and high evaporation rates due to enhanced surface air convergence over northeast South America and the tropical Atlantic Ocean. This was linked to negative sea surface temperature (SST) anomalies in the tropical Pacific and the anomalous ascending branch of an eastward shifted Walker Cell. These factors induced a meridional Hadley cell and enhanced subsidence over southeast South America, leading to reduced moisture convergence and precipitation.

In addition to these factors, the canonical La Niña event in the second semester of 2020 played a role in prolonging the dry conditions over South America. Previous studies, such as [32,33], had also discussed the influence of La Niña events on southern Brazil, highlighting the connection between canonical La Niña events and negative precipitation anomalies.

In fact, the majority of historical drought events in the SB region, including the 2020 event, are attributed to the ENSO phenomenon, particularly the La Niña phase, which is characterized by negative values of the Oceanic Niño Index (ONI). Additionally, Ref.[34] conducted a study in the Paraná River Basin using the SPI-12, which revealed that the highest percentage of the area affected by drought events (SPI-12 ≤ -1.00) was primarily observed during La Niña years (1984/85, 1988, 1999).

In the year 2020, neutral ENSO conditions prevailed in the first half of the year, followed by the onset of La Niña conditions during the JAS trimester, which persisted until the beginning of 2023.

## 4. Summary

The analysis of the SPI-3 series for the SB and SEB regions indicated a significant precipitation deficit throughout the year 2020, especially in the Autumn (MAM) and Spring (SON) months, where drought affected approximately 60% to 70% of the study area, classified as severe and extreme in all three datasets used (PERSIANN, CHIRPS, and ERA-5). The innovative S-TRACK method allowed for the construction of a spatial drought trajectory, revealing that this drought comprised three successive events. Initially, the onset of drought was observed at southern latitudes, with intensity ranging from moderate to extreme. As these events progressed northward, their intensity peaked at lower latitudes before dissipating or diminishing in intensity.

It is important to highlight that the persistence of drought areas in the same region over time contributed to the worsening severity of droughts during the MAM trimester, characterized by extreme drought events. Furthermore, the trajectories of drought events varied in extent, with the first event covering a considerable distance, while the second and third events had shorter trajectories. This variation in the extent of droughts may have significant implications for affected communities and water resource management.

In summary, the identification and characterization of drought-prone areas through the SPI-3 and S-TRACK methods represent a comprehensive and effective approach for integrated and sustainable resource management in the face of drought challenges. This enables the implementation of adaptive and mitigating strategies aimed at protecting ecosystems, socioeconomic activities, and the quality of life of local communities affected by the phenomenon.

**Author Contributions:** Conceptualization, Osmar Bonfim; Formal analysis, Rafael Maroneze; Investigation, Vanessa Ferreira; Methodology, Osmar Bonfim and Vanessa Ferreira; Resources, Roilan Valdes; Software, Osmar Bonfim and Rafael Maroneze; Supervision, Rafael Maroneze and Luca Mortarini; Visualization, Roilan Valdes; Writing – original draft, Osmar Bonfim and Vanessa Ferreira; Writing – review & editing, Luca Mortarini.

**Funding:** This research was funding by ENGIE Brasil Energia and Companhia Energética Estreito grant number P&D-00403-0054/2022.

**Acknowledgments:** This study has been developed as part of the Research and Technological Development Project of the Brazilian electrical energy sector, regulated by National Electric Energy Agency (ANEEL), having received from ENGIE Brasil Energia and Companhia Energética Estreito (P&D-00403-0054/2022).

**Conflicts of Interest:** The authors declare no conflicts of interest.

## References

1. DERAL – Departamento de Economia Rural. Boletim Informativo – Estiagem Histórica no Paraná. 2020. https://www.agricultura.pr.gov.br/sites/default/arquivos_restritos /files/documento/2020-05/estiagem_18_maio_2020.pdf. (Accessed May, 2023).
2. Getirana, A., Libonati, R., Cataldi, M. Brazil is in water crisis—it needs a drought plan. Nature , **2021**, 600(7888), 218-220. https://doi.org/10.1038/d41586-021-03625-w
3. Naumann, G., Podesta, G., Marengo, J., Luterbacher, J., Bavera, D., Arias-Muñoz, C., Marinho Ferreira Barbosa, P., Cammalleri, C., Chamorro, L., Cuartas, L.A., De Jager, A., Escobar, C., Hidalgo, C., Leal De Moraes, O.L., Mccormick, N., Maetens, W., Magni, D., Masante, D., Mazzeschi, M., Seluchi, M., De Los Milagros Skansi, M., Spinoni, J., Toreti, A. The 2019-2021 extreme drought episode in La Plata Basin, EUR 30833 EN, Publications Office of the European Union, Luxembourg, 2021. ISBN 978-92-76-47671-9, https://doi:10.2760/346183.
4. Gomes, M.S., de Albuquerque Cavalcanti, I.F., Müller, G.V. 2019/2020 drought impacts on South America and atmospheric and oceanic influences. Weather and Climate Extremes, **2021,** 34, 100404. https://doi.org/10.1016/j.wace.2021.100404.
5. Spinoni, J., Barbosa, P., De Jager, A., McCormick, N., Naumann, G., Vogt, J.V., Magni, D., Masante, D., Mazzeschi, M. A new global database of meteorological drought events from 1951 to 2016. Journal of Hydrology: Regional Studies, **2019**, 22, 100593. https://doi.org/10.1016/j.ejrh.2019.100593.

6. Diaz, V., Perez, G.A.C., Van Lanen, H.A., Solomatine, D., Varouchakis, E.A. An approach to characterize spatio-temporal drought dynamics. Advances in Water Resources, **2020**, 137, 103512. https://doi.org/10.1016/j.advwatres.2020.103512
7. Herrera-Estrada, J. E., Satoh, Y., Sheffield, J. Spatiotemporal dynamics of global drought. Geophysical Research Letters, **2017**, 44(5), 2254-2263. https://doi.org/10.1002/2016GL071768
8. Hosseini, A., Ghavidel, Y., Farajzadeh, M. Characterization of drought dynamics in Iran by using S-TRACK method. Theoretical and Applied Climatology, **2021**, 145(1-2), 661-671. https://doi.org/10.1007/s00704-021-03656-3
9. Verhoeven, E., Wardle, G.M., Roth, G.W., Greenville, A.C. Characterizing the spatiotemporal dynamics of drought and wet events in Australia. Science of The Total Environment, **2022**, 846, 157480. https://doi.org/10.1016/j.scitotenv.2022.157480.
10. Sadeghi, M., Nguyen, P., Naeini, M.R.., Hsu, K., Braithwaite, D., Sorooshian, S. PERSIANN-CCS-CDR, a 3-hourly 0.04° global precipitation climate data record for heavy precipitation studies. Sci Data, **2021**, 8, 157. https://doi.org/10.1038/s41597-021-00940-9
11. [11] Funk, C., Peterson, P., Landsfeld, M., Pedreros, D., Verdin, J., Shukla, S., ... & Michaelsen, J. The climate hazards infrared precipitation with stations—a new environmental record for monitoring extremes. Sci Data, **2015**, 2, 150066. https://doi.org/10.1038/sdata.2015.66
12. Hersbach, H., Bell, B., Berrisford, P., Hirahara, S., Horányi, A., Muñoz-Sabater, J., ... & Thépaut, J.N. The ERA5 global reanalysis. Quarterly Journal of the Royal Meteorological Society, **2020**, 146(730), 1999-2049. https://doi.org/10.1002/qj.3803
13. Tirivarombo, S., Osupile, D., Eliasson, P. Drought monitoring and analysis: Standardized Precipitation Evapotranspiration Index (SPEI) and Standardized Precipitation Index (SPI). Physics and Chemistry of the Earth, **2018**. https://doi.org/10.1016/j.pce.2018.07.001
14. [14] Kamruzzaman, M., Cho, J., Jang, M.W., Hwang, S. Comparative evaluation of standardized precipitation index (SPI) and effective drought index (EDI) for meteorological drought detection over Bangladesh. Journal of the Korean Society of Agricultural Engineers, **2019**, 61(1), 145-159. https://doi.org/10.5389/KSAE.2019.61.1.145
15. McKee, T.B., Doesken, N.J., Kleist, J. The relationship of drought frequency and duration to time scales. In: Proceedings of the 8th Conference on Applied Climatology. AMS, Boston, MA, **1993**, p. 179–184.
16. Rocha, L.H.D.S., Silva, D.F.D., Kayano, M.T., Bonfim, O.E.T. Homogeneidade, Eventos Extremos e suas Causas Climáticas: Bacia Hidrográfica do Rio São Francisco. Revista Brasileira de Meteorologia, **2022**, 37, 199-212. https://doi.org/10.1590/0102-77863710122
17. Dos Santos, B.C., Sanches, R.G., Moreira, R.M., Bourscheidt, V., Souza, P.H. Análise espaço-temporal da precipitação na região central do estado de São Paulo utilizando dados CHIRPS. Revista Brasileira de Geografia Física, **2022**, 15(05), 2582-2600. https://doi.org/10.26848/rbgf.v15.5.p2582-2600
18. Taylor, K.E. Summarizing multiple aspects of model performance in a single diagram. Journal of Geophysical Research, **2001**, 106, 7183–7192. https://doi.org/10.1029/2000JD900719
19. Yang, X., Zhou, B., Xu, Y., Han, Z. CMIP6 evaluation and projection of temperature and precipitation over China. Advances in Atmospheric Sciences, **2021**, 38, 817-830. https://doi.org/10.1007/s00376-021-0351-4
20. Diaz, V., Corzo Perez, G.A., Van Lanen, H.A.J., Solomatine, D. Intelligent drought tracking for its use in machine learning: implementation and first results. In: La Log- gia, G., Freni, G., Puleo, V., De Marchis, M. (Eds.), HIC 2018. 13th International Conference on Hydroinformatics, 3 Palermo: EasyChair , 2018. https://doi.org/10. 29007/klgg.
21. Diaz, V., Perez, G.A.C., Van Lanen, H.A., Solomatine, D., Varouchakis, E.A. Characterisation of the dynamics of past droughts. Science of the Total Environment, **2020b**, 718, 134588. https://doi.org/10.1016/j.scitotenv.2019.134588
22. Corzo Perez, G.A., Van Huijgevoort, M.H.J., Voß, F., Van Lanen, H.A.J. On the spatio-temporal analysis of hydrological droughts from global hydrological models. Hydrology and Earth System Sciences, **2011**, 15(9), 2963-2978. https://doi.org/10.5194/hess-15-2963-201
23. Anjum, M.N., Irfan, M., Waseem, M., Leta, M.K., Niazi, U.M., ... & Nadeem, M.U. Assessment of PERSIANN-CCS, PERSIANN-CDR, SM2RAIN-ASCAT, and CHIRPS-2.0 rainfall products over a semi-arid subtropical climatic region. Water, **2022**, 14(2), 147. https://doi.org/10.3390/w14020147
24. Prakash, S. Performance assessment of CHIRPS, MSWEP, SM2RAIN-CCI, and TMPA precipitation products across India. Journal of hydrology, **2019**, 571, 50-59. https://doi.org/10.1016/j.jhydrol.2019.01.036
25. Singh, T., Saha, U., Prasad, V.S., Gupta, M.D. Assessment of newly-developed high resolution reanalyses (IMDAA, NGFS and ERA5) against rainfall observations for Indian region. Atmospheric Research, **2021**, 259, 105679. https://doi.org/10.1016/j.atmosres.2021.105679.

26. Jafarpour, M., Adib, A., Lotfirad, M. Improving the accuracy of satellite and reanalysis precipitation data by their ensemble usage. Applied Water Science, **2022**, 12(9), 232. https://doi.org/10.1007/s13201-022-01750-z
27. Coelho, C., Uvo, C., Ambrizzi, T. Exploring the impacts of the tropical Pacific SST on the precipitation patterns over South America during ENSO periods. Theor Appl Climatol, **2002**, 71, 185–197. https://doi.org/10.1007/s007040200004
28. [28] Minuzzi, R.B., Sediyama, G.C., Ribeiro, A., Costa, J. El Niño: ocorrência e duração dos veranicos do Estado de Minas Gerais. Revista brasileira de engenharia agrícola e ambiental, **2005**, 9, 364-371. https://doi.org/10.1590/S1415-43662005000300011
29. Cemadem - Centro Nacional de Monitoramento e Alertas de Desastres Naturais. Boletim Monitoramento de secas e impactos no Brasil Abril/2020. Ministério da Ciência, Tecnologia e Inovações. 2020. http://www2.cemaden.gov.br/wp-content/uploads/2020/05/ Boletim_BRASIL_abr2020.pdf (Accessed May, 2023).
30. Marengo, J.A., Cunha, A.P., Cuartas, L.A., Deusdará Leal, K.R., Broedel, E., Seluchi, M. E., ... & Bender, F. Extreme drought in the Brazilian Pantanal in 2019–2020: characterization, causes, and impacts. Frontiers in Water, **2021**, 3, 639204. https://doi.org/10.3389/frwa.2021.639204
31. Geirinhas J.L., Russo A., Libonati R., Miralles, D., Ramos, A., Gimeno, L., & Trigo, R. Combined large-scale tropical and subtropical forcing on severe soil desiccation in South America. Research Square, **2023**. https://doi.org/10.21203/rs.3.rs-2732119/v1
32. Tedeschi, R.G., Cavalcanti, I.F.A., Grimm, A.M. Influences of two types of ENSO on South American precipitation. International Journal of Climatology, **2013**. https://doi.org/10.1002/joc.3519
33. Grimm, A.M., Almeida, A.S., Beneti, C.A.A., Leite, E.A. O efeito combinado de oscilações climáticas na produção de extremos: a seca de 2020 no Sul do Brasil. RBRH, **2020**, 25. https://doi.org/10.1590/2318-0331.252020200116
34. Santos, E.B., de Freitas, E.D., Rafee, S.A.A., Fujita, T., Rudke, A.P., Martins, L.D., Souza, R.A.F., Martins, J. A. Spatio-temporal variability of wet and drought events in the Paraná River basin—Brazil and its association with the El Niño—Southern oscillation phenomenon. International Journal of Climatology, **2021**, 41(10), 4879-4897. https://doi.org/10.1002/joc.7104